Supersonic Cold Spraying for Zeolitic Metal-Organic Framework Films

Do-Yeon Kim,[1,†] Bhavana N. Joshi,[1,†] Jong-Gun Lee,[1] Jong-Hyuk Lee[1], Ji Sun Lee,[2] Young Kyu Hwang,[2] Jong-San Chang,[2,3] Salem Al-Deyab,[4] Jin-Chong Tan,[5,*] Sam S. Yoon[1,*]

[1]School of Mechanical Engineering, Korea University, Seoul 136-713, Republic of Korea
[2]Res. Group for Nanocatalysts, Korea Res. Inst. of Chem. Tech., Daejeon 305-600, Republic of Korea
[3]Dept of Chem., Sungkyunkwan University, Suwon 440-476, Republic of Korea
[4]Petrochem. Research Chair, Dept. of Chem., King Saud Univ., Riyadh 11451, Saudi Arabia
[5]Department of Eng. Science, University of Oxford, Parks Road, Oxford OX1 3PJ, United Kingdom

Abstract

We describe the first use of high-rate supersonic spray coating to deposit thin films of ZIF-8, a zeolitic metal-organic framework (MOF), adopting a sodalite architecture. This cold-spray technique is versatile and scalable, with tunable processing parameters capable of generating either a textured crystalline film or a randomly oriented polycrystalline coating on both metallic and non-metallic substrates. We provide evidence that guest occupancy by organic solvents (dimethylformamide, dimethylacetamide, and dimethylsulfoxide) in the sodalite cage of ZIF-8 structurally stabilizes the framework against high-velocity impact, resulting in the preferred orientations observed. Moreover, we show that amorphous ZIF-8 films can be straightforwardly obtained at high air pressure exceeding 7 bars in which the particle velocity is ~500 m/s. It is anticipated that this high-throughput approach can be adapted to fabricate microstructurally compact and strongly adhered ZIF-8 films.

[†]Equal contribution

[*]Corresponding authors: jin-chong.tan@eng.ox.ac.uk, skyoon@korea.ac.kr

Introduction

Metal-organic frameworks (MOFs) are extensively studied as a new class of multifunctional materials in materials science and chemistry [1]. In MOFs, metal atoms are coordinated with organic ligands to form diverse crystalline 3D frameworks. The structures of MOFs can be dense or porous; MOFs of specific structures can be used in many applications such as gas separation, sensing, catalysis, optoelectronics, and magnetism [2-4]. Zeolitic imidazolate frameworks (ZIFs) [5] comprise an important subclass of MOFs closely related to zeolitic silica polymorphs as per their chemical bonding (Si-O-Si); [6] they typically consist of divalent metal cations (e.g., M = Zn^{2+}, Co^{2+}) solely coordinated by the nitrogen atoms of the imidazolate (Im) bridging ligand (M-Im-M), forming microporous crystalline lattices. In the ZIF family, ZIF-8 contains Zn(II) metal ions connected by 2-methylimidazolate (mIm) organic linkers, resulting in periodic frameworks of $Zn(mIm)_2$. ZIF-8 has been extensively studied for its tunable pore size, chemical stability, and thermal robustness [7, 8]. The topology of ZIF-8 corresponds to that of the zeolite sodalite [9], which can be described as a space-filling packing of truncated octahedra. In particular, ZIF-8 crystallizes as a cubic lattice (space group $I\bar{4}3m$) containing cavities with diameters of 11.6 Å, connected via six-membered ring apertures with 3.5 Å windows and four-ring apertures [10]. The good thermal and chemical stability of ZIF-8 [11], combined with the regular pore architecture and long-range ordering of the structure, has motivated extensive research in the fields of membrane science, gas storage, drug delivery, and catalysis [12-14]. With respect to mechanical stability, the crystal structures of ZIFs are more flexible than the analogous aluminosilicate zeolites [15]; hence, they can undergo structural transformations and are susceptible to collapse under the application of either low pressure (0.34 GPa) [16] or temperature (300˚C) [6].

The deposition of MOF thin films and surface coatings is under intense study because of the many possible applications of thin-film MOFs in optical, electronic, and energy harvesting devices [17]. MOF applications would greatly increase if a high-throughput facile processing route were developed to fabricate MOFs as supported homogenous thin films. Despite numerous studies, the majority of reported techniques are not ideal for commercial manufacturing and production scale-up [2, 14] [4] [18]. The most common methods of MOF film deposition are summarized below. Secondary growth is one of these methods, entailing a stepwise deposition in which the first step deposits a seed layer and the second step grows further layers by solvothermal synthesis and dip-coating from solutions [19]. Another method is *in situ* crystallization, where the ZIF layer is grown on a bare substrate by solvothermal synthesis. Crystal orientation can affect the properties of the membranes or films, depending on the applications. Secondary growth is useful to control the crystal orientation of the MOF films [20]. Highly oriented ZIF-8 films were prepared by Bux *et al.* [19] on alumina discs *via* the secondary growth method. In the first step, they deposited a seed layer by dip-coating using a mixture of ZIF-8 nanocrystals dispersed in water/polyethylenimine (PEI); the seed layer was treated solvothermally to grow the films. They reported the growth of crystalline ZIF-8 films with highly oriented (100) planes after 2 h of deposition; these membranes showed improved performance in H_2/hydrocarbon separation over typical ZIF-8 films. A set of *b*-oriented (010) and *c*-oriented (002) ZIF-L membranes was prepared by Zhong *et al*. [20] employing the secondary growth method for gas permeation. The *b*-oriented films were grown from an *in situ* seed layer by dip coating on porous alumina. They used seeded alumina for three rounds of secondary growth by the same method to grow *b*-oriented ZIF-L films. For the *c*-oriented films, ZIF-L crystals dispersed in PEI were vacuum-filtered onto porous alumina as a seed layer. Using the secondary growth method, *c*-oriented ZIF-L membranes were prepared by dip coating for 30 min. The gas permeation properties of the *c*-oriented ZIF-L membranes were

reported as better than those of the *b*-oriented ZIF-L membranes. Cookney *et al*. [13] reported the synthesis of ultrathin ZIF-8 nanofilms on silicon by stepwise dip-coating. The films were morphologically dense and homogenous, with crystallinity oriented towards the (112) plane. Recently, Papporello *et al*. [21] deposited ZIF-8 films on both metallic and nonmetallic substrates utilizing different solvent media by the solvothermal method. They grew (200)- and (110)-oriented ZIF-8 films on copper using a mixed solvent of methanol and acetate, and then prepared structured catalysts based on the films. Hence, the fabrication of oriented ZIF thin films is important for selective gas separation [19, 20], structured catalysts [21], and optical applications [3].

While some recent reports describe the application of spray-type processing strategies to fabricate MOF films, the approach we describe in the current study is distinct from those found in the literature. Melgar *et al*. [22] reported the direct spraying of ZIF-7 membranes by electrospraying on an alumina disk, where the membrane thickness was controlled by changing the electrospray solution flow rate and deposition time. These ZIF-7 membranes showed H_2 permeability and H_2/CO_2 separation capacity. Likewise, Fan *et al*. [23] used a simultaneous spray self-assembly approach in order to increase the ZIF-8 particle loading while maintaining a uniform dispersion. They synthesized ZIF-8/Polydimethylsiloxane (PDMS) composite membranes on polysulfone for butanol pervaporation. Sanchez and co-workers [24] reported the application of spray-drying to make multicomponent MOF hollow superstructures. Arsnal *et al*. also used a spray process to grow highly oriented crystalline HKUST-1 MOFs on modified Au substrates [25].

We report a new method for the deposition of MOF films by cold-spraying colloidal ZIF-8 sol. The cold-spraying technique is a high-rate coating method in which particles are injected into a supersonic gas stream, created by the expansion of a compressed gas through a

convergent-divergent de Laval nozzle. The particles, accelerated to supersonic velocities, possess sufficient kinetic energy to bond to the substrate upon impact. Other technical details of the cold-spraying apparatus have been discussed in earlier reports [26]. The cold-spraying technique utilizes the high kinetic impact energy of the high-velocity particles to promote strong bonding between the substrate and the particles. Herein, we demonstrate that the cold-spray coating method is effective in successfully depositing ZIF-8 films that maintain the original crystal structure of the source nanoparticles. Furthermore, we observed the deposition of ZIF-8 films with (112)-oriented crystal structures in the presence of 20% dimethylformamide (DMF) in the colloidal sol. To the best of our knowledge, this is the first report on the deposition of oriented ZIF-8 films by supersonic spraying. This work provides new insight on the deposition of ZIF-8 films and the mechanical responses of the films to high-speed impact, and describes the tailoring of the crystallographic orientations and crystallinity of the deposited MOF films.

Experimental

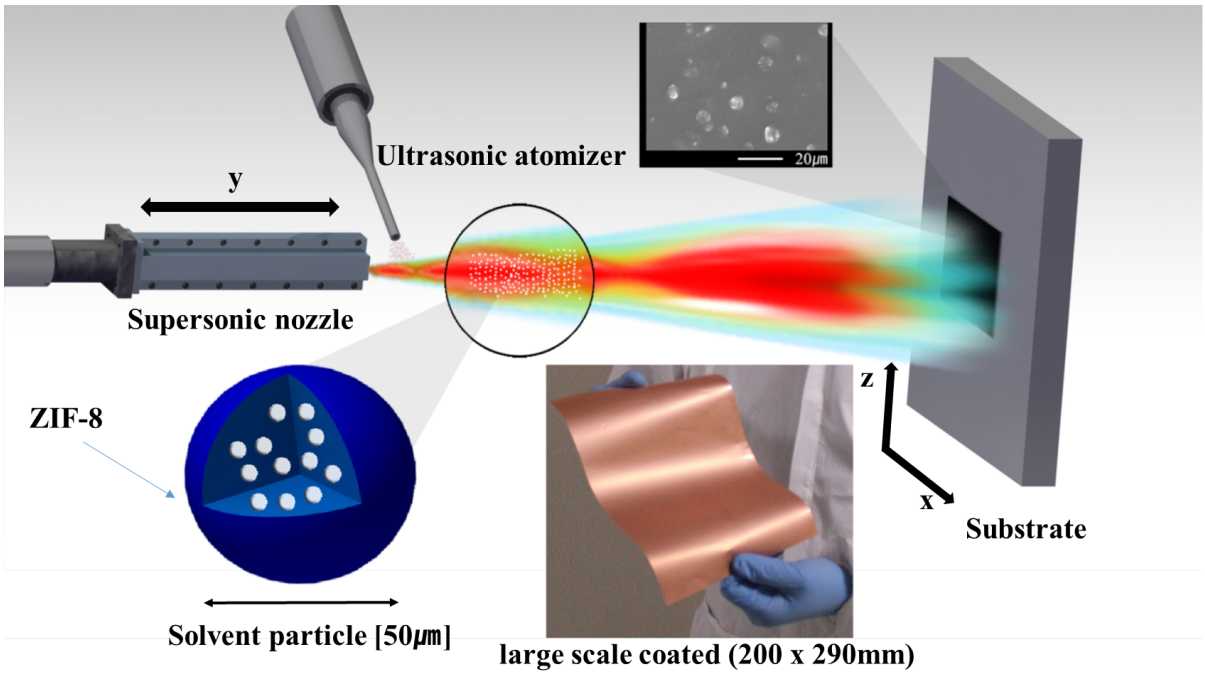

Figure 1 Schematic of the custom-built supersonic spray-coating system.

Crystalline ZIF-8 was synthesized by the microwave-irradiation method. Typically, 2-methylimidazole (663 mg, 8 mmol) and $Zn(NO_3)_2$・6H2O (304 mg, 1 mmol) were mixed in a Teflon vessel with a 28 mL of methanol and then the solution mixture was reacted at 150 °C for 1h. After cooled down to room temperature, the products were purified by centrifugation and then washed with methanol three times to remove unreacted reactants. Finally, the products were dried overnight below 100 °C in atmosphere.

The synthesized ZIF-8 powder with nanoparticles of 100–150 nm diameter was used. The films were deposited using a supersonic spray-coating system (also known as cold-spray method), shown schematically in **Figure 1**. The system consists of a gas tank, gas heater, supersonic nozzle, ultrasonic liquid processor, syringe pump, and XY translation stage, configured as shown in **Figure 1**, and as described in a previous paper [27]. In order to deposit the ZIF-8 films, a colloidal solution was prepared using 50 mL isopropyl alcohol (IPA), 10 mL

N,*N*-dimethylformamide (DMF), 6 wt.% of nylon-6, and 1 g of ZIF-8 powder. Nylon was included to promote the adhesion of the ZIF-8 particles to the substrates. The DMF was added to the solution in order to enhance the dispersion of the ZIF-8 nanoparticles. A sonicator (Pronextech, South Korea) was used for 2 min to create the dispersion of ZIF-8. This solution was then pumped by a syringe pump (KDS LEGATO 100) towards the nozzle *via* the ultrasonic liquid processor (VCS134ATFT, Sonic & Materials, Inc., USA). The feed solution was discharged in an undifferentiated, supersonic air stream through the nozzle, which accelerated the sol toward the substrate; a uniform coating was generated by four cycles of supersonic particle deposition. The operating air pressure (P_0) varied from 2–7 bar and the heater temperature for the air was varied from 150–350°C. The ZIF-8 films were coated on both copper and glass substrates with an average thickness of 20 μm (see **Figure S1**). The ZIF-8 nanoparticles gained high kinetic energy by the hot compressed air blown through the supersonic nozzle, which yielded well-adhered compact ZIF-8 films on the substrates.

Results and Discussion

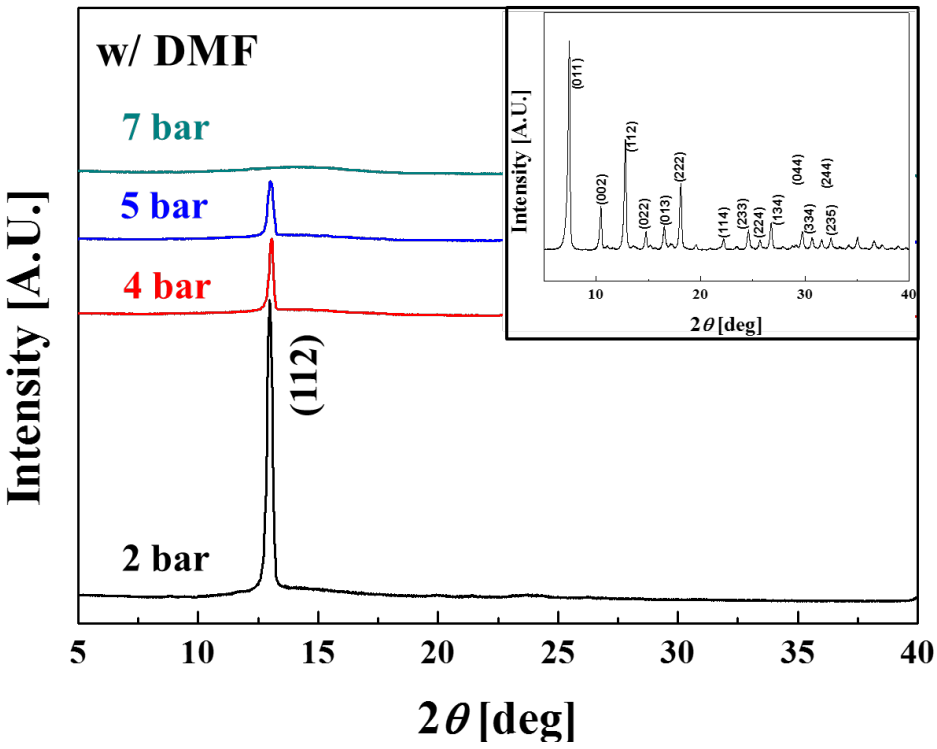

Figure 2. Pressure-dependent XRD patterns of ZIF-8 films deposited on a copper substrate with air gas temperature of 250°C. The inset shows the XRD pattern of the raw ZIF-8 powder.

The ZIF-8 films were deposited by supersonic spraying onto glass and copper substrates. **Figure 2** shows the X-ray diffraction (XRD) patterns of the ZIF-8 films deposited on copper substrates, recorded with an X-ray diffractometer (SmartLab, Rigaku). The XRD pattern of the raw ZIF-8 powder [12] (see inset **Figure 2**) shows dominant Bragg peaks (2θ) at 7.31, 10.24, 12.65, 16.03, and 17.84°, corresponding to the respective crystallographic planes. However, the same ZIF-8 powder after deposition in the presence of DMF in sol shows a dominant peak at ~12.7°, assigned to the (112) plane, as shown in **Figure 2**. A similar orientation was established in the film deposited on glass, as shown in the supporting information (**Figure S2)**. We reasoned that this change in crystal orientation is connected to the presence of occluded DMF in the sol; the possible mechanism responsible for this effect is

elucidated below. In addition, we expect that the (112)-oriented ZIF-8 films are dense in nature because of the presence of DMF and compaction by impact pressure between the substrate and the particles during deposition. Recently Cookney *et al*. [13] reported a similar type of (112)-oriented ZIF-8 thin films deposited by dip-coating on silicon; the films were observed to be dense in terms of surface morphology and were evacuated to access the void space in ZIF-8.

In this study, the peak consistently appears at $2\theta = 12.7°$ for the films deposited at 2 bar, 4 bar, and 5 bar. However, the intensity of the peaks decreases with increasing air pressure, which we attribute to the lattice strain in the compacted films accompanied by a gradual loss in long-range ordering (crystallinity). At ~7 bar, the sharp peak disappears, suggesting the amorphization of the ZIF-8 structure by porous framework collapse. Similar high-pressure amorphization of ZIF-8 has been reported by Chapman *et al*. [28] under hydrostatic compression and also observed through mechanical impacts from ball milling by Bennett *et al*. [29]. Notably, in the case of cold-spray coatings, the increase in air pressure from 2 bar to 7 bar increases the velocity of air, as well as that of the sol particles, from 310 to 400 m/s, thus increasing the impact pressure against the substrate. To estimate this effect, we solved the 1D isentropic equation; the relationship of temperature *vs.* velocity is shown in **Figure 3.**

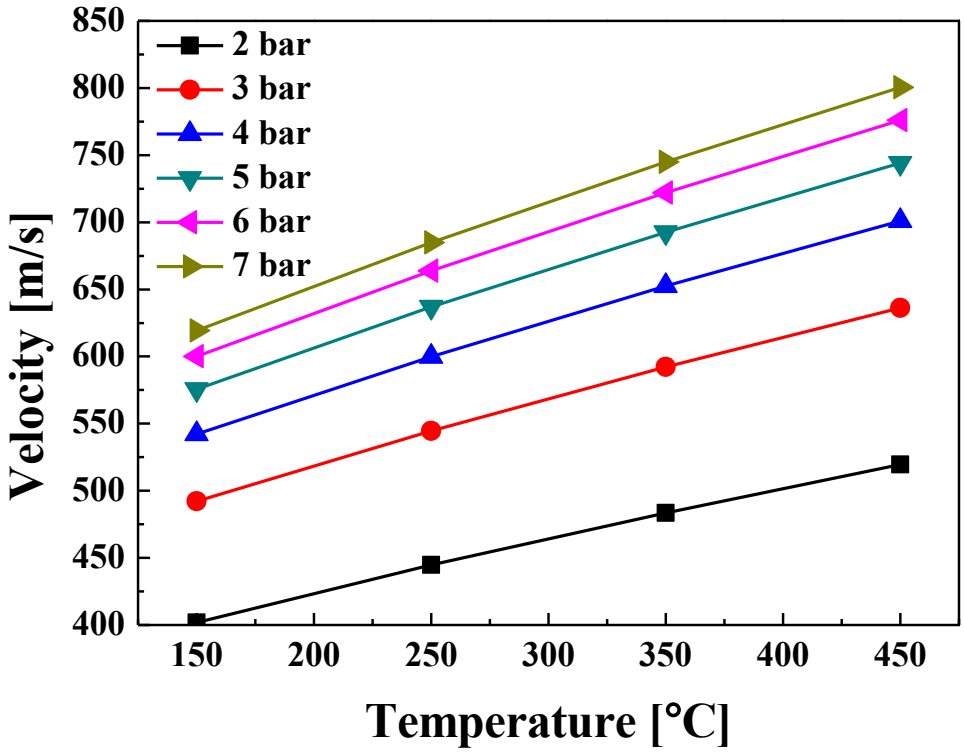

Figure 3. Plot of temperature *vs.* velocity at different air pressures, as simulated from 1D isentropic equation

We previously reported a high-impact-pressure study on inorganic materials, describing the effect of impact pressure on the fracture and adhesion of the particles on the substrate [30]. High kinetic energy of the cold spray was acquired by converting the pressure and temperature of the upstream chamber through a De Laval nozzle. The pressures used here for the flow of particles are not very high, especially at 2 to 5 bar, but at sufficiently high air temperatures in the chamber ($T \geq 250$°C), the velocity of particles increases, which could generate high impact pressures. Thus, at increased air temperatures ($T = 250$°C) and pressures from 2 to 7 bar, the velocity of the particles is expected to be ~500 m/s, which ultimately increases the impact pressure of the particles striking the substrate. This process leads to particle fracture and the

destabilization of the ZIF-8 frameworks [15], causing the structural amorphization we observed at high pressures exceeding 7 bars (see **Figure 2**).

Under the assumption of a 1D isentropic flow (inviscid and adiabatic), the exit velocity V_e of the air can be estimated using the equation below:

$$V_e = \sqrt{2c_p T_o [1 - (P_e / P_o)^{(\gamma-1)/\gamma}} \quad (1)$$

where c_p is the specific heat, T_0 and P_0 are the chamber temperature and pressure and P_e is the exit pressure, respectively. V_e was multiplied by a factor of 0.8 to estimate the particle velocity V_p (i.e., $V_p \sim 0.8V_e$), based on the Stokes number computation. For the V_p estimation, one may find the two limiting cases of the Stokes number (*Stk*) based on the minimum and maximum particle sizes present within the supersonic gas stream. A blob of liquid of ~50 μm comprising numerous ZIF-8 particles is the maximum size present when it is injected into the supersonic stream. This liquid blob becomes fragmented; eventually only the ZIF-8 primary particles remain before they strike the substrate, because all liquid has evaporated before reaching the substrate; this latter scenario provides the other limiting end case with a minimum size of ~0.1 μm. The Stokes numbers of these minimum-sized particles, defined as the ratio of particle response time (τ_p) to the surrounding flow characteristic time (τ_g), are fairly small (*Stk* < 2), in which case the particle velocity approaches the gas velocity; see **Fig. 5** of Ref. [31]. Note that the gas exit velocity was estimated using Eq. (1) above with the chamber pressure and temperature of P_0 = 2 bar and T_0 = 250°C, respectively. From this estimation, it is likely that the particles were accelerated to the gas velocity and retained sufficient momentum to be deposited onto the substrate with no evidence of waste or deflection from the substrate, which we confirmed experimentally. No wetting was observed at the substrate throughout the coating process, confirming the complete evaporation of the carrier liquids at the instant of particle

impact. It is also possible that the presence of the bow-shock would hinder the adhesion of the particles on the substrate. However, such hindrance was not significant in our case, as we did not observe evidence of fragmented debris of the particles or wasted precursor in the coating area.

Table 1. The maximum and minimum Stokes number estimation for determining the particle velocity range at chamber conditions of P_0 = 2 bar and T_0 = 250°C.

	ρ_p [g/cm^3]	D [cm]	μ_g [g/cm s]	d [cm]	V_e [m/s]	$\tau_p=\rho_p D^2/(18\mu_g)$ [µs]	$\tau_g=d/V_e$ [µs]	$Stk=\tau_p/\tau_g$
Max.	0.786	0.05	2.485	0.8	445	44	1.8	2.44
Min.	7.14	0.0001	2.485	0.8	445	0.0016	1.8	$8.8\cdot10^{-5}$

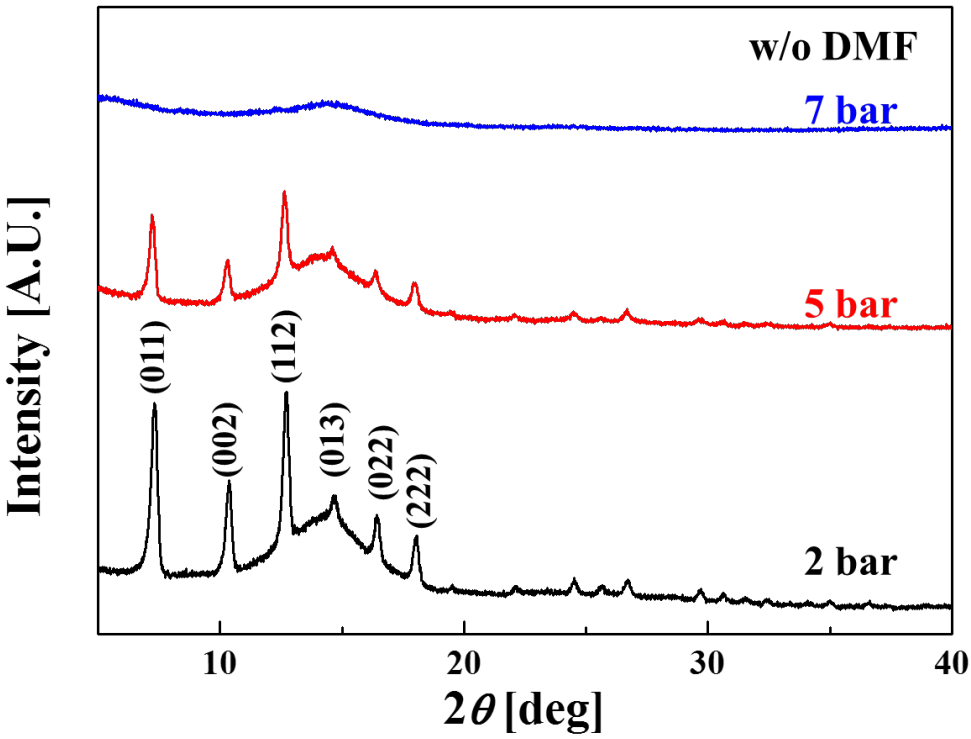

Figure 4. XRD patterns of ZIF-8 films on copper substrates without DMF in solution. The operating gas temperature was 250°C.

In order to confirm the effect of DMF in modifying the orientation of ZIF-8, as well as to study the effect of pressure, films were spray-deposited at different pressures with no DMF in the sol. The experimental process was similar to the aforementioned procedure, except that DMF was excluded from the solution. The ZIF-8 films were deposited on copper substrates. The XRD patterns of the non-DMF films deposited at different pressures are presented in **Figure 4**. The peaks corresponding to the planes (011), (002), (112), (013), (022), and (222) are clearly observed in all films, similar to the pattern from ZIF-8 powder, albeit with lower intensities. Interestingly, no preferential film orientation is observed when no DMF is used in spraying. However, similar to the case using DMF, the amorphization of films occurs at the air pressure of 7 bar. From this result, it is clear that the presence of DMF in sol is significant in generating the orientation of the spray-deposited ZIF-8 films.

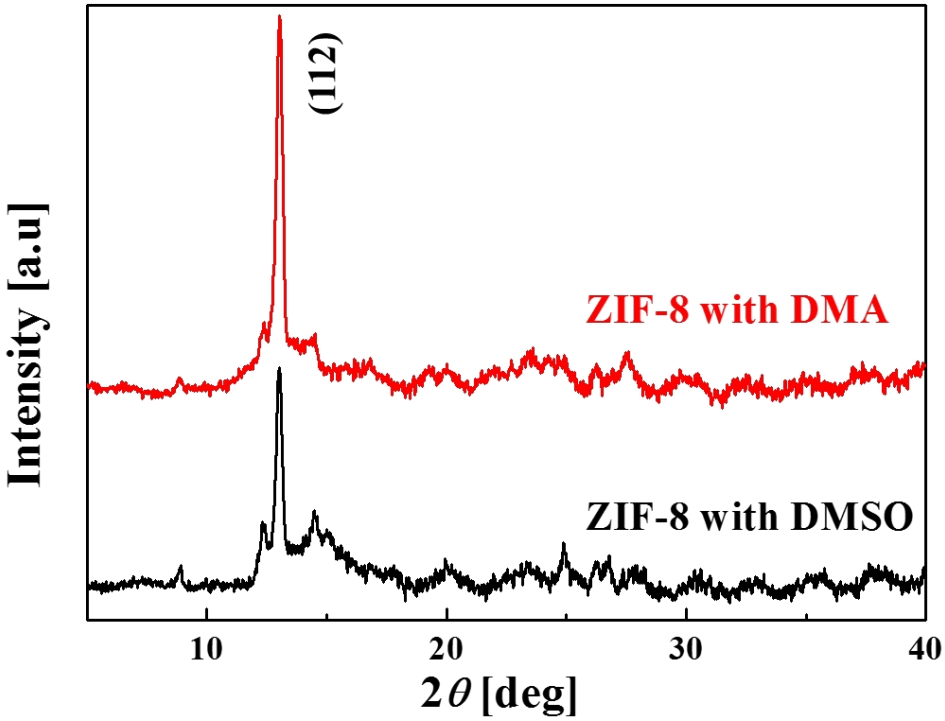

Figure 5. XRD patterns of ZIF-8 film deposited using DMSO and DMA as substitutes for DMF in the sol. The operating gas pressure and temperature were 2 bar and 250°C, respectively.

We have postulated that the presence of high-boiling-point occluded molecules in ZIF-8 pores (herein, DMF with a boiling point of ~150°C) could mechanically stabilize the flexible sodalite framework structure [9], thereby reducing the likelihood of impact-induced amorphization. We tested this hypothesis by replacing DMF with two other high-boiling-point solvents: dimethylacetamide (DMA, boiling point ~165°C) and dimethylsulfoxide (DMSO, ~189°C). Significantly, both experiments result in predominant (112) diffraction peaks, reminiscent of that obtained using DMF (see **Figure 5**). In contrast, we reasoned that the low-boiling-point IPA (~83°C) without DMF, as in **Figure 4**, would be rapidly volatized in flight by the high temperature of the air stream, meaning that IPA would not be available to mechanically stabilize the ZIF-8 pores during impact; thus, relatively greater amorphization was induced, as compared to the case with DMF from **Figure 2**. While guest-induced

hydrostatic stabilization against MOF structural collapse has been reported recently using a few common solvents [32, 33], this phenomenon has not yet been observed under a high-strain-rate dynamic impact scenario, as demonstrated in this work.

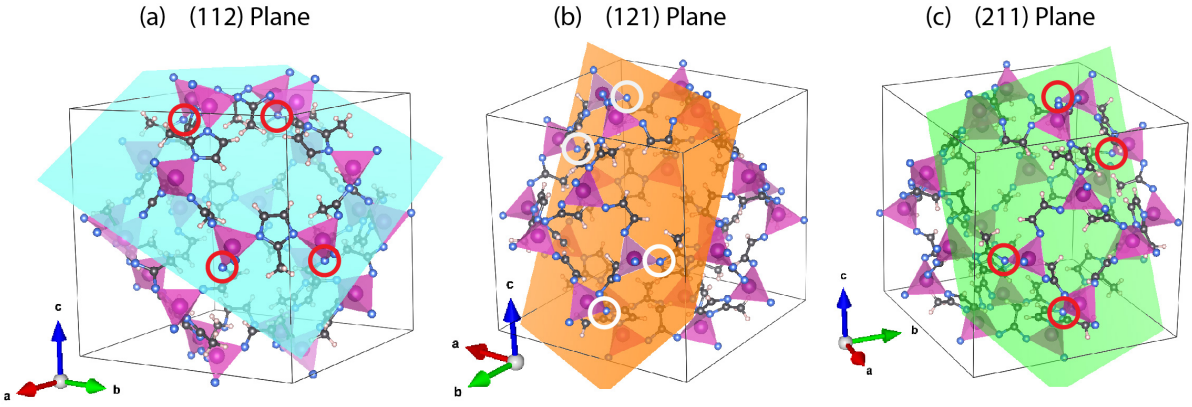

Figure 6. Potential cleavage planes identified in the cubic ZIF-8 unit cell (one sodalite cage; the nanosized pore is located in the middle), belonging to the {112}-oriented family of lattice planes. Examples depicted here are (a) (112), (b) (121), and (c) (211); not shown are the other 18 planes in this family such as (-1 1 2), (1 2 -1), (-2 1 1), (-2 1 -1), etc. The purple tetrahedra represent ZnN_4 coordination sites. The circle markers designate weak points at the vertices of ZnN_4 sites susceptible to rupture by shear stresses. Color code: purple = zinc, gray = carbon, blue = nitrogen, and white = hydrogen.

To elucidate the existence of the preferred (112) film orientation, examination of the detailed crystal configuration of the ZIF-8 unit cell is necessary. **Figure 6** shows that the {112}-oriented planes are formed by the intersection of four nitrogen atoms connected to four different tetrahedral ZnN_4 coordination sites in each sodalite cage of ZIF-8, indicating that these are effectively cleavage planes susceptible to crystallographic fracture triggered by (sliding) shear stresses [9] from high-energy impact. In fact, {112}-oriented planes are prevalent in ZIF-8; altogether, there are 21 such planes per unit cell (**Figure 6**). From this analysis, we assume that the probability of slicing through one such cleavage plane is equal to

that of crystal fracture; this selective rupturing mechanism could yield the major intensity in the (112) preferred orientation observed in the XRD data shown in **Figure 2**.

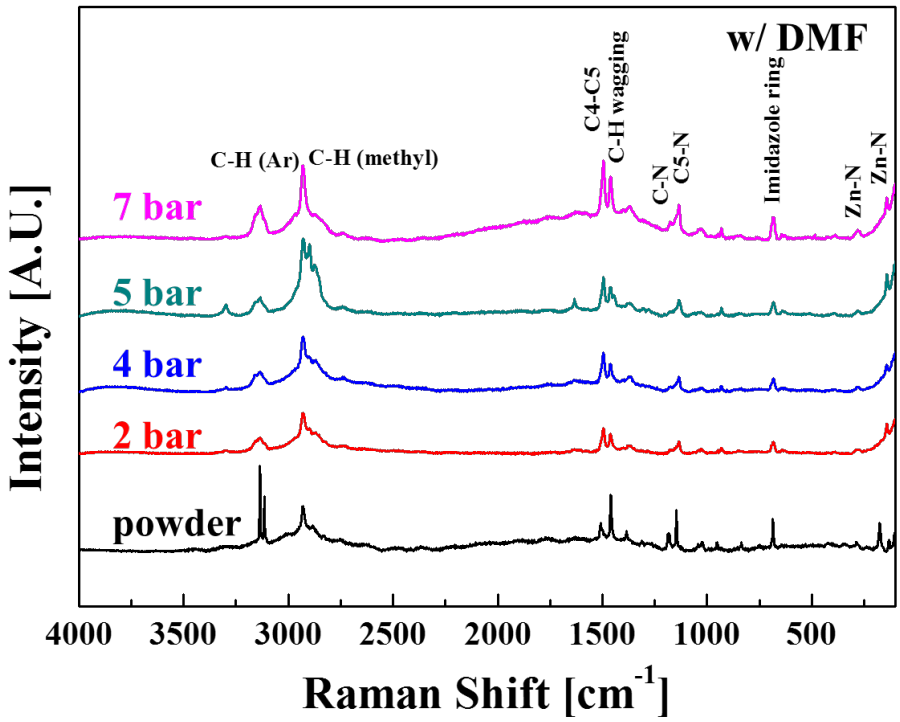

Figure 7. Pressure-dependent Raman spectra of ZIF-8 films with DMF at 250 °C air gas temperature.

Table 2. Raman frequencies and band assignments

Wavenumber [cm^{-1}]	Band assignment
178	Zn-N
273	Zn-N
686	Imidazole ring
1143	C5-N
1186	C-N
1458	C-H wagging
1508	C4-C5
2915	C-H (methyl)
3115	C-H(Ar)
3134	C-H(Ar)

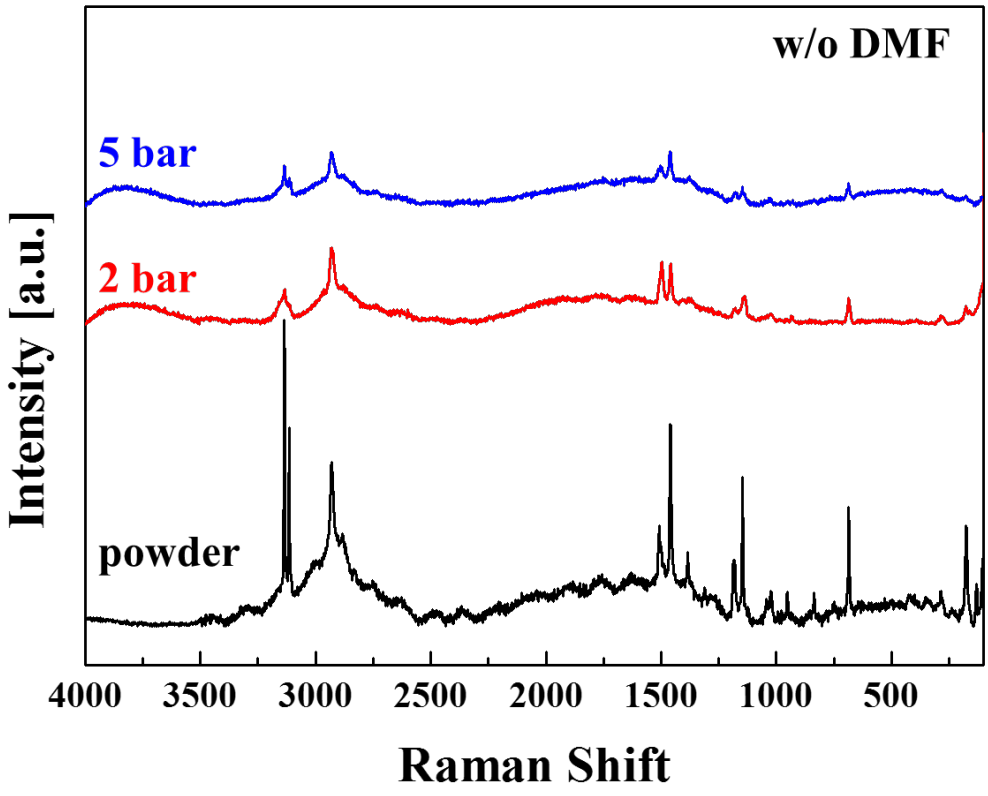

Figure 8. Pressure-dependent Raman spectra without DMF in solution

The Raman spectra of ZIF-8 films deposited at different pressures, showing dominant intense bands corresponding to the vibrations of methyl groups and imidazole rings, are presented in **Figure 7**. The Raman spectra presented here are from films deposited with DMF in sol. Bands are observed at 178 and 273 cm^{-1}, 686 cm^{-1}, 1143 cm^{-1}, and 1458 cm^{-1}, corresponding to Zn−N stretching, imidazole ring vibration, C5−N stretching, and methyl bending, respectively. A comparison of the ZIF-8 Raman data with results reported by Gayatri *et al*. [34] shows that the peaks agree well with the literature, which verifies that the coated films are indeed ZIF-8. The peak locations and respective band assignments are listed in **Table 2**. Ryder *et al.* [15] also reported similar vibrational frequencies of organic and Zn-N bonds in ZIF-8 using high-resolution inelastic neutron-scattering measurements. The Raman spectrum of ZIF-8 powder is also presented in **Figure 7.** The Raman spectra of the films deposited at different gas pressures without DMF in sol are presented in **Figure 8**, showing that all Raman

bands remain similar without shifting. This Raman data confirm that the chemical structure of ZIF-8 in the absence and presence of DMF remains unchanged.

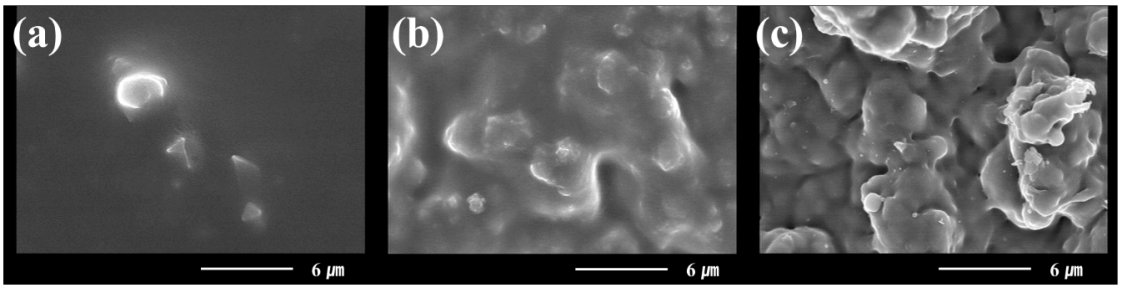

Figure 9 SEM images of ZIF-8 films with DMF deposited at (a) 2 bar, (b) 5 bar, and (c) 7 bar. The operating gas temperature was T = 250°C.

The morphologies of the ZIF-8 films were inspected by scanning electron microscopy (SEM). **Figure 9** shows the SEM images of the ZIF-8 films deposited on a copper substrate with DMF in sol. In **Figure 9(a)**, a thin layer is observed, covering the ZIF-8 grains with a smooth surface of DMF residues. However, the surface texture is clearly roughened in the higher-pressure films in **Figure 9 (b) and (c)**, showing more violent fragmentation of the particles at higher impact speeds. In order to analyze the elemental details of the film, energy dispersive X-ray spectroscopy (EDX) data were obtained. The presence of Zn, O, and C is confirmed, as shown in **Table 3**.

Table 3. Elemental details of the ZIF-8 film fabricated at the operating gas temperature and pressure of 250˚C and 4 bar, respectively.

Elements	Weight[%]	Atomic[%]
C K	47.76	70.18
O K	18.85	20.80
Zn L	33.39	9.02
Total	100	100

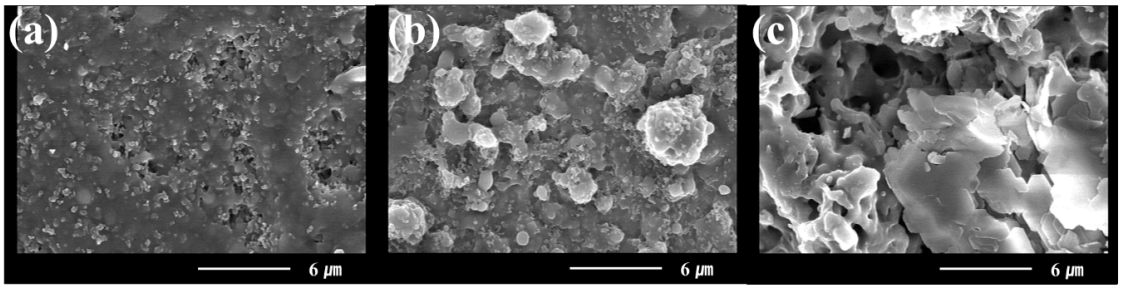

Figure 10 SEM images of ZIF-8 films without DMF deposited at (a) 2 bar, (b) 5 bar, and (c) 7 bar. The operating gas temperature is T = 250°C.

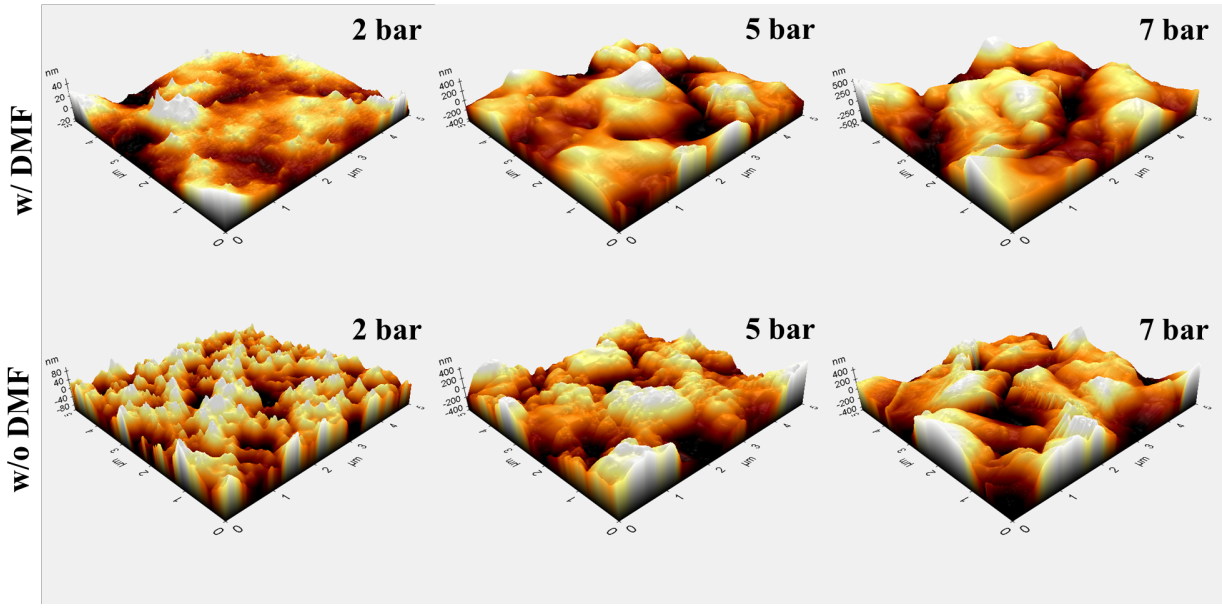

Figure 11 AFM of ZIF-8 films deposited (upper row) with and (lower row) without DMF.

The SEM images of films deposited without DMF, shown in **Figure 10**, depict more porous and more agglomerated surface microstructures. These rougher surfaces confirm that DMF inclusion induces the smoother surface texture shown in **Figure 9**. The dark and bright areas show the porosity of the film surfaces of ZIF-8 in the films deposited at 2 and 5 bar. Meanwhile, the amorphous films deposited at 7 bar exhibit flat surfaces of the ZIF-8 particles.

The surface topographies of the films were characterized by atomic force microscopy (AFM). The 3D AFM surface morphologies of the ZIF-8 films deposited at 250°C gas temperature and varied pressures are shown in **Figure 11**. The upper and lower rows show

films made *with* and *without* DMF in sol, respectively. The AFM analysis shows peaks and valleys, associated with the random lateral stacking of ZIF-8 nanoparticles. The films clearly show increasing surface roughness with violent particle fragmentation at higher pressures, resulting from the increased impact energy of cold-spray deposition.

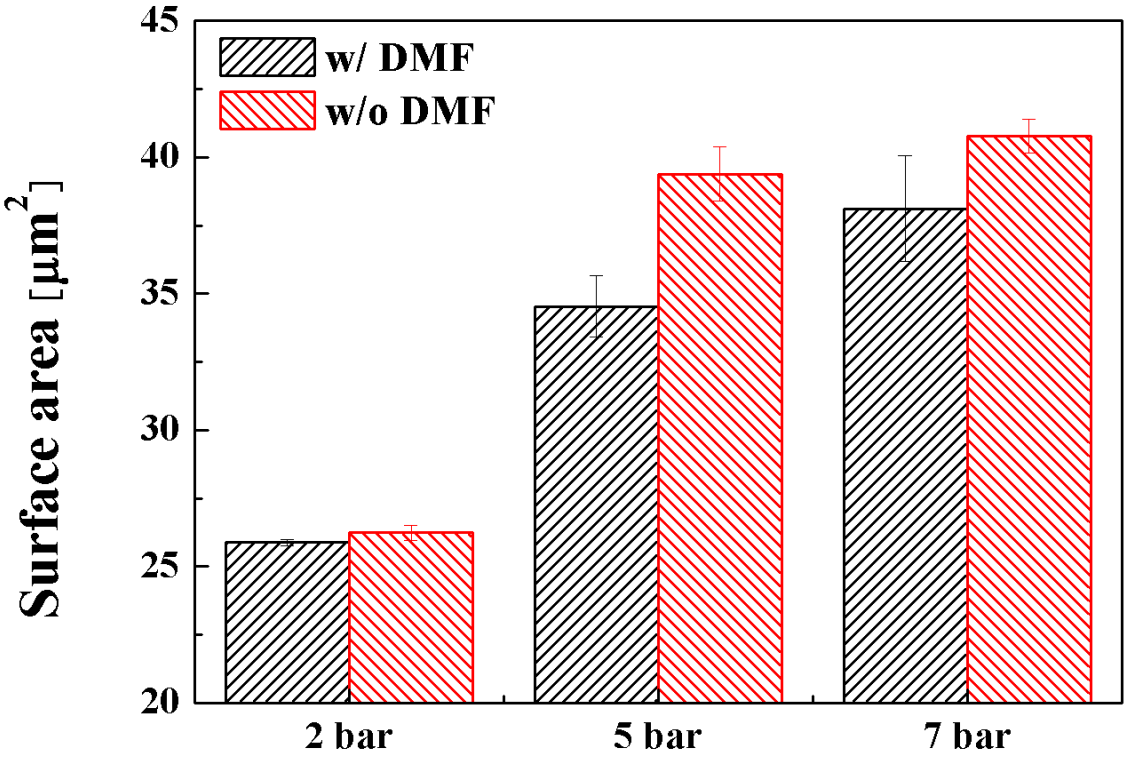

Figure 12 Surface areas of ZIF-8 films deposited with and without DMF at 250°C air gas temperature

The surface areas of the films deposited with and without DMF, as determined from AFM [35], are presented in **Figure 12**. The films deposited at 2 bar show similar surface areas, relatively higher than that of the uncoated copper substrate with surface area 25 μm^2. The surface areas increase with increasing air pressure, because of the fracture of the particles deposited at higher impact velocities. However, the surface areas of the films created with DMF

are consistently lower than those made without, verifying the SEM images in **Figure 9** that show the surface covering of nylon and DMF.

Conclusion

Polycrystalline ZIF-8 powder is transformed by cold-spraying deposition to (112)-oriented ZIF-8 films with guest-induced structural stabilization caused by occluded solvent molecules in the MOF pores (e.g., DMF, DMA, DMSO). This is the first attempt to deposit preferentially oriented and non-oriented MOF films by supersonic spray coating, a highly promising technique ideal for size scaling and high-throughput commercialization. Notably, in the absence of DMF, it is also possible to deposit ZIF-8 films maintaining the original (random) polycrystalline structure of the ZIF-8 nanoparticles. This study has elucidated the formation of ZIF-8 films by spray deposition, including the mechanical behavior of nanoparticles at high-rate impact, showing that the gas pressure used in cold-spray coating can be tuned to control the crystallinity and surface microstructures of the resultant films. The deposition process of preferentially oriented films presents a new strategy for manipulating the crystal structures and physical properties of ZIF-8 films. The preparation of amorphous ZIF films by high-rate supersonic spraying is also of significant interest in the production of chemically functionalizable hybrid glass materials [33]. Finally, the versatility and scalability of the proposed manufacturing approach indicate that it may be easily adapted to fabricate large-scale ZIF-8 films for practical and commercial applications. Certainly, the efficacy of the supersonic spraying methodology bodes well for follow-on studies to ascertain the performance of the deposited films for specific MOF applications [2-4], ranging from gas separations and catalysis to optoelectronics and sensors.

References

[1] P. Silva, S.M.F. Vilela, J.P.C. Tome, F.A. Almeida Paz, Multifunctional metal-organic frameworks: from academia to industrial applications, Chemical Society Reviews 44 (2015) 6774-6803.

[2] O. Shekhah, J. Liu, R.A. Fischer, C. Wöll, MOF thin films: existing and future applications, Chemical Society Reviews 40 (2011) 1081-1106.

[3] J.C. Tan, J.D. Furman, A.K. Cheetham, Relating Mechanical Properties and Chemical Bonding in an Inorganic− Organic Framework Material: A Single− Crystal Nanoindentation Study, Journal of the American Chemical Society 131 (2009) 14252-14254.

[4] P. Falcaro, R. Ricco, C.M. Doherty, K. Liang, A.J. Hill, M.J. Styles, MOF positioning technology and device fabrication, Chemical Society Reviews 43 (2014) 5513-5560.

[5] A. Phan, C.J. Doonan, F.J. Uribe-Romo, C.B. Knobler, M. O'Keeffe, O.M. Yaghi, Synthesis, Structure, and Carbon Dioxide Capture Properties of Zeolitic Imidazolate Frameworks, Accounts of Chemical Research 43 (2010) 58-67.

[6] T.D. Bennett, A.L. Goodwin, M.T. Dove, D.A. Keen, M.G. Tucker, E.R. Barney, A.K. Soper, E.G. Bithell, J.-C. Tan, A.K. Cheetham, Structure and properties of an amorphous metal-organic framework, Physical review letters 104 (2010) 115503.

[7] H.-L. Jiang, B. Liu, T. Akita, M. Haruta, H. Sakurai, Q. Xu, Au@ZIF-8: CO Oxidation over Gold Nanoparticles Deposited to Metal−Organic Framework, Journal of the American Chemical Society 131 (2009) 11302-11303.

[8] F. Rashidi, C.R. Blad, C.W. Jones, S. Nair, Synthesis, characterization, and tunable adsorption and diffusion properties of hybrid ZIF-7-90 frameworks, AIChE Journal 62 (2016) 525-537.

[9] J.-C. Tan, B. Civalleri, C.-C. Lin, L. Valenzano, R. Galvelis, P.-F. Chen, T.D. Bennett, C. Mellot-Draznieks, C.M. Zicovich-Wilson, A.K. Cheetham, Exceptionally Low Shear Modulus in a Prototypical Imidazole-Based Metal-Organic Framework, Physical review letters 108 (2012) 095502.

[10] Y. Hu, H. Kazemian, S. Rohani, Y. Huang, Y. Song, In situ high pressure study of ZIF-8 by FTIR spectroscopy, Chem. Commun. 47 (2011) 12694-12696.

[11] K.S. Park, Z. Ni, A.P. Côté, J.Y. Choi, R. Huang, F.J. Uribe-Romo, H.K. Chae, M. O'Keeffe, O.M. Yaghi, Exceptional chemical and thermal stability of zeolitic imidazolate frameworks, Proceedings of the National Academy of Sciences 103 (2006) 10186-10191.

[12] S.R. Venna, J.B. Jasinski, M.A. Carreon, Structural evolution of zeolitic imidazolate framework-8, Journal of the American Chemical Society 132 (2010) 18030-18033.

[13] J. Cookney, W. Ogieglo, P. Hrabanek, I. Vankelecom, V. Fila, N.E. Benes, Dynamic response of ultrathin highly dense ZIF-8 nanofilms, Chemical Communications 50 (2014) 11698-11700.

[14] M.D. Allendorf, V. Stavila, Crystal engineering, structure–function relationships, and the future of metal–organic frameworks, CrystEngComm 17 (2015) 229-246.

[15] M.R. Ryder, B. Civalleri, T.D. Bennett, S. Henke, S. Rudić, G. Cinque, F. Fernandez-Alonso, J.-C. Tan, Identifying the Role of Terahertz Vibrations in Metal-Organic Frameworks: From Gate-Opening Phenomenon to Shear-Driven Structural Destabilization, Physical review letters 113 (2014) 215502.

[16] T.D. Bennett, P. Simoncic, S.A. Moggach, F. Gozzo, P. Macchi, D.A. Keen, J.-C. Tan, A.K. Cheetham, Reversible pressure-induced amorphization of a zeolitic imidazolate framework (ZIF-4), Chemical Communications 47 (2011) 7983-7985.

[17] V. Stavila, A.A. Talin, M.D. Allendorf, MOF-based electronic and opto-electronic devices, Chem. Soc. Rev. 43 (2014) 5994-6010.

[18] A. Bétard, R.A. Fischer, Metal–Organic Framework Thin Films: From Fundamentals to Applications, Chemical Reviews 112 (2012) 1055-1083.

[19] H. Bux, A. Feldhoff, J. Cravillon, M. Wiebcke, Y.-S. Li, J. Caro, Oriented Zeolitic Imidazolate Framework-8 Membrane with Sharp H2/C3H8Molecular Sieve Separation, Chemistry of Materials 23 (2011) 2262-2269.

[20] J.Y. Zhaoxiang Zhong, Rizhi Chen, Zexian Low, Ming He,Jefferson Zhe Liuc and Huanting Wang, Oriented two-dimensional zeolitic imidazolate framework-L membranes and their gas permeation properties†, Journal of Materials Chemistry A 3 (2015) 15715-15722.

[21] R.L. Papporello, E.E. Miró, J.M. Zamaro, Secondary growth of ZIF-8 films onto copper-based foils. Insight into surface interactions, Microporous and Mesoporous Materials 211 (2015) 64-72.

[22] V.M. Aceituno Melgar, H.T. Kwon, J. Kim, Direct spraying approach for synthesis of ZIF-7 membranes by electrospray deposition, Journal of Membrane Science 459 (2014) 190-196.

[23] H. Fan, Q. Shi, H. Yan, S. Ji, J. Dong, G. Zhang, Simultaneous Spray Self-Assembly of Highly Loaded ZIF-8-PDMS Nanohybrid Membranes Exhibiting Exceptionally High Biobutanol-Permselective Pervaporation, Angewandte Chemie International Edition 53 (2014) 5578-5582.

[24] A. Carné-Sánchez, I. Imaz, M. Cano-Sarabia, D. Maspoch, A spray-drying strategy for synthesis of nanoscale metal–organic frameworks and their assembly into hollow superstructures, Nature chemistry 5 (2013) 203-211.

[25] H.K. Arslan, O. Shekhah, J. Wohlgemuth, M. Franzreb, R.A. Fischer, C. Wöll, High-Throughput Fabrication of Uniform and Homogenous MOF Coatings, Advanced Functional Materials 21 (2011) 4228-4231.

[26] D.-Y. Kim, J.-J. Park, J.-G. Lee, D. Kim, S.J. Tark, S. Ahn, J.H. Yun, J. Gwak, K.H. Yoon, S. Chandra, S.S. Yoon, Cold Spray Deposition of Copper Electrodes on Silicon and Glass Substrates, Journal of thermal spray technology 22 (2013) 1092-1102.

[27] D.Y. Kim, S. Sinha-Ray, J.J. Park, J.G. Lee, Y.H. Cha, S.H. Bae, J.H. Ahn, Y.C. Jung, S.M. Kim, A.L. Yarin, Self-Healing Reduced Graphene Oxide Films by Supersonic Kinetic Spraying, Advanced Functional Materials 24 (2014) 4986-4995.

[28] K.W. Chapman, G.J. Halder, P.J. Chupas, Pressure-Induced Amorphization and Porosity Modification in a Metal−Organic Framework, Journal of the American Chemical Society 131 (2009) 17546-17547.

[29] T.D. Bennett, S. Cao, J.C. Tan, D.A. Keen, E.G. Bithell, P.J. Beldon, T. Friscic, A.K. Cheetham, Facile Mechanosynthesis of Amorphous Zeolitic Imidazolate Frameworks, Journal of the American Chemical Society 133 (2011) 14546-14549.

[30] J.-G. Lee, D.-Y. Kim, B. Kang, D. Kim, S.S. Al-Deyab, S.C. James, S.S. Yoon, Thin film metallization by supersonic spraying of copper and nickel nanoparticles on a silicon substrate, Computational Materials Science 108 (2015) 114-120.

[31] M. Lee, J. Park, D. Kim, S. Yoon, H. Kim, D. Kim, S. James, S. Chandra, T. Coyle, J. Ryu, Optimization of supersonic nozzle flow for titanium dioxide thin-film coating by aerosol deposition, Journal of Aerosol Science 42 (2011) 771-780.

[32] A.J. Graham, A.-M. Banu, T. Düren, A. Greenaway, S.C. McKellar, J.P.S. Mowat, K. Ward, P.A. Wright, S.A. Moggach, Stabilization of Scandium Terephthalate MOFs against Reversible Amorphization and Structural Phase Transition by Guest Uptake at Extreme Pressure, Journal of the American Chemical Society 136 (2014) 8606-8613.

[33] T.D. Bennett, J. Sotelo, J.-C. Tan, S.A. Moggach, Mechanical properties of zeolitic metal–organic frameworks: mechanically flexible topologies and stabilization against structural collapse, CrystEngComm 17 (2015) 286-289.

[34] G. Kumari, K. Jayaramulu, T.K. Maji, C. Narayana, Temperature Induced Structural Transformations and Gas Adsorption in the Zeolitic Imidazolate Framework ZIF-8: A Raman Study, The Journal of Physical Chemistry A 117 (2013) 11006-11012.

[35] F. Macht, K. Eusterhues, G.J. Pronk, K.U. Totsche, Specific surface area of clay minerals: Comparison between atomic force microscopy measurements and bulk-gas (N2) and -liquid (EGME) adsorption methods, Applied Clay Science 53 (2011) 20-26.